PTEP

Prog. Theor. Exp. Phys. **2012**, 02B010 (16 pages)
DOI: 10.1093/ptep/pts023

Beam and SKS spectrometers at the K1.8 beam line

Toshiyuki Takahashi[1], Satoshi Adachi[2], Michelangelo Agnello[3], Kanae Aoki[1], Osamu Araoka[1], Bernd Bassalleck[4], Elena Botta[5,8], Stefania Bufalino[5,8], Nobuyuki Chiga[6], Petr Evtoukhovitch[7], Alessandro Feliciello[8], Juergen Franz[9], Hiroyuki Fujioka[2], Shuhei Hayakawa[10], Erina Hirose[1], Ryotaro Honda[6], Kenji Hosomi[6], Yudai Ichikawa[2], Youichi Igarashi[1], Masahisa Iida[1], Masahiro Ikeno[1], Kenta Itahashi[11], Naoya Ishibashi[10], Shigeru Ishimoto[1], Ruri Iwasaki[1], Yutaka Kakiguchi[1], Katsuyu Kasami[1], Sunji Kim[12], Ryuta Kiuchi[12], Takeshi Koike[6], Yusuke Komatsu[13], Alexandr Kustov[7], David Mjavia[7], Yasuhiro Makida[1], Simonetta Marcello[5,8], Tomofumi Maruta[14], Shinichi Masumoto[13], Kenji Matsuoka[10], Koji Miwa[6], Anatolii Moiseenko[7], Manabu Moritsu[2], Tomofumi Nagae[2], Megumi Naruki[1], Hiroyuki Noumi[15], Hirokazu Ohhata[1], Takahiro Okamura[1], Ryosuke Ota[10], Masatoshi Saito[1], Atsushi Sakaguchi[10], Valentin Samoilov[7], Misako Sato[6], Yoshinori Sato[1], Michiko Sekimoto[1], Yoshihisa Shirakabe[1], Kotaro Shirotori[15], Hitoshi Sugimura[2], Shoji Suzuki[1], Yoshihiro Suzuki[1], Hitoshi Takahashi[1], Tomonori N. Takahashi[11], Hirokazu Tamura[6], Manobu Tanaka[1], Kazuya Tauchi[1], Toshiyuki Tanaka[10], Kiyoshi Tanida[12], Atsushi O. Tokiyasu[2], Kotaro Yoshida[10], Akihisa Toyoda[1], Zviadi Tsamalaidze[7], Tomohisa Uchida[1], Mifuyu Ukai[6], Hiroaki Watanabe[1], Takeshi O. Yamamoto[6], Yoshio Yonemoto[6], Choong-Jae Yoon[15]

[1]*Institute of Particle and Nuclear Studies (IPNS), High Energy Accelerator Organization (KEK), Tsukuba, Ibaraki 305-0801, Japan*
[2]*Department of Physics, Kyoto University, Kyoto 606-8502, Japan*
[3]*Dipartimento Scienza Applicata e Tecnologia, Politecnico di Torino, 24 Torino, Italy*
[4]*Department of Physics and Astronomy, The University of New Mexico, Albuquerque, NM 87131-0001, USA*
[5]*Dipartmento di Fisca, Universitá di Torino, Torino I-10125, Italy*
[6]*Department of Physics, Tohoku University, Sendai 980-8578, Japan*
[7]*Joint Institute for Nuclear Reserch, Dubna, Moscow Region 141980, Russia*
[8]*INFN, Sezione di Torino, Torino I-10125, Italy*
[9]*Fakultät für Physik, University of Freiburg, Freiburg D-79104, Germany*
[10]*Department of Physics, Osaka University, Toyonaka, Osaka 560-0043, Japan*
[11]*RIKEN Nishina Center for Accelerator-Based Science, RIKEN, Wako, Saitama 351-0198, Japan*
[12]*Department of Physics and Astronomy, Seoul National University, Seoul 151-747, Korea*
[13]*Department of Physics, The University of Tokyo, Bunkyo, Tokyo 113-0033, Japan*
[14]*J-PARC Center, Japan Atomic Energy Agency (JAEA), Tokai, Ibaraki 319-1195, Japan*
[15]*Research Center for Nuclear Physics (RCNP), Osaka University, Ibaraki, Osaka 567-0047, Japan*

Received May 30, 2012; Accepted July 18, 2012; Published October 9, 2012

High-resolution spectrometers for both incident beams and scattered particles have been constructed at the K1.8 beam line of the Hadron Experimental Facility at J-PARC. A point-to-point optics is realized between the entrance and exit of *QQDQQ* magnets for the beam spectrometer. Fine-pitch wire chamber trackers and hodoscope counters are installed in the beam spectrometer to accept a high rate beam up to 10^7 Hz. The superconducting kaon spectrometer for scattered particles was transferred from KEK with modifications to the cryogenic system and detectors. A missing-mass resolution of $1.9 \pm 0.1\,\mathrm{MeV}/c^2$ (FWHM) was achieved for the Σ peaks of $(\pi^{\pm}, K^{+})$ reactions on a proton target in the first physics run of E19 in 2010.

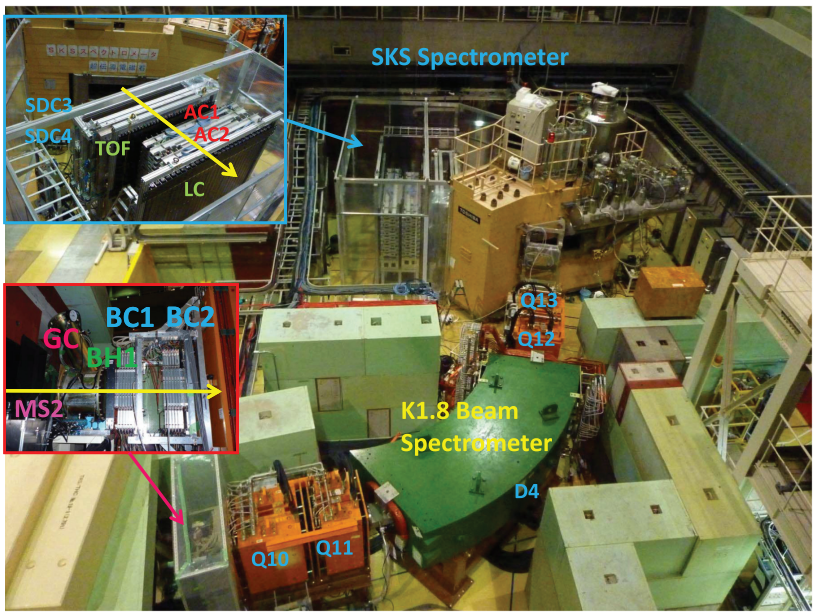

Fig. 1. Photograph of the K1.8 experimental area of the J-PARC Hadron Experimental Facility in November 2009. Insets show photographs of the upstream part of the beam spectrometer and the downstream part of the SKS. Q10–13 and D4 are beam spectrometer magnets. MS2 is the second mass slit of the K1.8 beam line. BC1, BC2, SDC3, and SDC4 are tracking wire chambers. BH1 and TOF are scintillators, while GC, AC1,2, and LC are Čerenkov counters for triggers and particle identification.

1. Introduction

One of the main topics of research at the J-PARC Hadron Facility is strangeness nuclear physics. A lot of experiments on hypernuclear and strangeness physics using high-intensity meson beams such as kaons and pions have been proposed and are intended to take new data. As described in Ref. [1] in this special volume, the K1.8 beam line provides a high-intensity and high-purity K^- beam with a maximum momentum of 2.0 GeV/c. The 1.8 GeV/c K^- beam intensity is expected to be 1.9×10^6 [ppp] when the Ni production target is irradiated by 30 GeV primary protons of 2×10^{14} [ppp]. Kaon purity, $K^-/(\pi^- + \mu^-)$, is expected to be 3.5. In addition to high-intensity beams, two high-resolution spectrometers, a beam spectrometer for beam particles and a superconducting kaon spectrometer (SKS) [2] for scattered particles, are instrumented on the K1.8 beam line. Therefore, the K1.8 beam line facility is the most suitable to carry out high-resolution missing-mass spectroscopy of hypernuclei both for $S = -1$ and -2 [3,4] and that of exotic hadrons [5]. Coincidence measurements such as γ-ray spectroscopy [6] and weak decay experiments [7,8] can also be performed by employing high-intensity beams and the large solid-angle acceptance of SKS.

The construction of the K1.8 beam line and spectrometers was completed in 2009 (Fig. 1). Commissioning of the beam line and spectrometers commenced in October and November 2009. In November and December 2010, the first physics run of E19 (a search for the pentaquark, Θ^+ via the $p(\pi^-, K^-)$ reaction) [9] was carried out. In this article, basic instruments at the K1.8 beam line, the beam and SKS spectrometers with a data acquisition (DAQ) system, are described in detail. Most of the descriptions are updated from the previous report [10] with consideration of the results of the beam commissioning and the first physics run of E19.

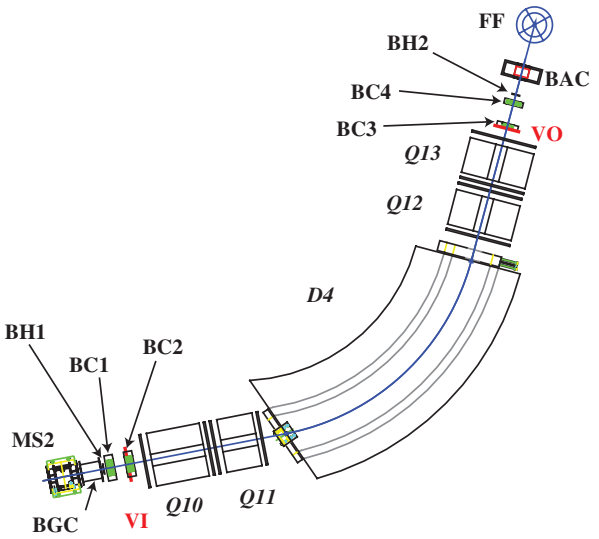

Fig. 2. Schematic drawing of the beam spectrometer of the K1.8 beam line. Q10–14 and D4 are beam spectrometer magnets. MS2 is the second mass slit of the K1.8 beam line. VI and VO mean the virtual plane of the entrance and exit of the *QQDQQ* system for the transport matrix. FF is the final focus point where an experimental target is set. BH1 and BH2 are plastic scintillators. BGC and BAC are gas and aerogel Čerenkov counters for triggers and particle identification. BC1–4 are tracking wire chambers.

2. Beam spectrometer

The beam spectrometer of the K1.8 beam line consists of a *QQDQQ* magnetic system, tracking wire chambers, and trigger counters as shown in Fig. 2. A vacuum chamber and ducts are installed in the magnet region. The vacuum windows where the beam passes through are made of 0.1 mm SUS. The *QQDQQ* magnetic system is designed to utilize point-to-point optics from the upstream (VI, 40 cm to the Q10 pole edge) and downstream (VO, 30 cm from the Q13 pole edge) points. Therefore, the multiple scattering at the entrance and exit of the *QQDQQ* does not affect the momentum resolution to the first order. The first-order optics parameters from VI to VO are -0.53, -0.84, and 1.61 cm/%, for horizontal (dispersive) magnifications, vertical magnifications, and dispersion, respectively. The momentum resolution is expected to be 3.3×10^{-4} (FWHM) when the position is measured with an accuracy of 0.2 mm (rms).

Beam trajectories are measured by wire chambers at both the entrance (BC1 and BC2) and the exit (BC3 and BC4) of the *QQDQQ* system for momentum and reaction vertex reconstructions. The straight lines of the entrance and exit are connected using a third-order transport matrix, and the momentum ($\delta = dp/p$) is determined. The magnetic field of the D4 magnet is monitored using a high-precision Hall probe (Digital Teslameter 151 by Group-3). The monitored data are recorded with time-stamps during the data-taking period for a time-dependent correction in the offline analysis.

2.1. Trigger and particle identification counters

Plastic scintillator hodoscopes are installed upstream of BC1 (BH1) and downstream of BC4 (BH2) for time-of-flight measurement with a flight length of 10.4 m, where the difference is 1.3 ns between 1.8 GeV/c kaons and pions. BH1 is divided horizontally into 11 segments with an equal thickness of 5 mm and different widths of 8, 12, 16, and 20 mm, so as to have almost equal beam rates. Phototubes with three-stage boosters (H1650MOD) are connected to both ends of each segment. The effective

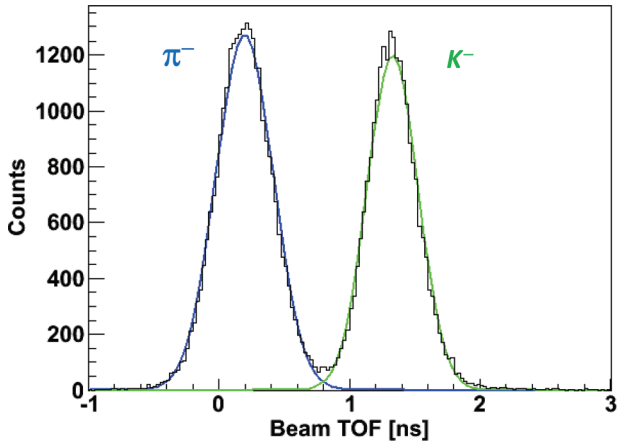

Fig. 3. Time-of-flight spectrum between BH1 and BH2 at 1.8 GeV/c.

area of BH1 is $170^{\mathrm{H}} \times 66^{\mathrm{V}}$ mm^2. BH2 is also horizontally segmented into 7 pieces of 5 mm thickness and different widths of 15, 20, and 30 mm. The effective area is $133^{\mathrm{H}} \times 60^{\mathrm{V}}$ mm^2. It also uses H1650MOD phototubes on both ends of each segment.

Each segment of BH1 and BH2 overlaps with its adjacent segment to avoid a dead space. However, we found from the first physics run in 2010 that the overlapping configuration of BH2 is not suitable for high-resolution missing-mass spectroscopy experiments. The energy loss of a particle that passes through the overlapping region becomes larger than that for a particle that passes through the single segment. This causes the offline analysis to be sophisticated and difficult. Therefore, we modified BH2 not to be overlapping in January 2012.

The resolution on the measured time-of-flight between BH1 and BH2 was approximately 140 ps (rms) after the pulse-height time-walk correction. Figure 3 shows the beam time-of-flight spectrum for 1.8 GeV/c particles, which was measured during a beam line study for kaon beam tuning. Kaons and pions are clearly separated.

A gas Čerenkov counter (BGC) is necessary for pion beam experiments in order to reject electrons (or positrons) in the beam. It is installed at the most upstream end of the beam spectrometer, in a very narrow space between the second mass slit (MS2) and BH1. The radiator is isobutane gas of 0.15 MPa. An aluminum mirror is coated with MgF_2, which is transparent to the UV photons. Čerenkov photons are detected by a phototube with a UV-transparent window (R1250-03). The measured number of photo-electrons was approximately 5 for higher than 0.5 GeV/c electrons. The efficiency was found to be 99.5%, enough to reject undesired electrons (or positrons) existing in the proportion of 12%–14% in the pion beam.

For kaon (K^-) beam experiments, an aerogel Čerenkov counter (BAC) is installed just upstream of the experimental target. The radiator is silica aerogel with a refractive index of 1.03 and dimensions of $230^{\mathrm{H}} \times 80^{\mathrm{V}} \times 66^{\mathrm{T}}$ mm^3. The inside of the box is covered with Teflon as a reflector. Signals from three phototubes (H6614-70UV) are summed up by a linear amplifier and processed for trigger logic, timing (TDC), and charge (ADC) readouts. At the optimum threshold setting during kaon beam tuning, we evaluated the BAC efficiency for pions, kaons, and protons: it turned out to be 99.99%, 8%, and 3%, respectively. The sensitivity for kaons and protons may be due to a small yield of scintillation from the Teflon reflectors and δ-ray electrons.

Table 1. Specifications of MWPC (BC1 and BC2) and drift chambers for the beam and SKS spectrometers.

Name	Eff. Area H × V (mm)	Anode pitch or drift distance	Planes	Tilted angle (X,U,V) (°)	Comments
BC1	256 × 100	1 mm pitch	X-V-U-X-V-U	0, +15, −15	New
BC2	256 × 100	1 mm pitch	V-U-X-V-U-X	0, +15, −15	New
BC3	192 × 150	1.5 mm	X-X′-U-U′-V-V′	0, +15, −15	New
BC4	240 × 150	2.5 mm	U-U′-V-V′-X-X′	0, +15, −15	K6 BDC
SDC1	192 × 150	1.5 mm	V-V′-U-U′	+15, −15	New
SDC2	400 × 150	2.5 mm	V-V′-U-U′-X-X′	0, +15, −15	New
SDC3	2140 × 1140	10 mm	V-X-U-V-X-U	0, +30, −30	AGS-D6 BD
SDC4	2140 × 1140	10 mm	V-X-U-V-X-U	0, +30, −30	AGS-D6 BD

The following logic determines beam pions or kaons in the online triggers and scaler counts:

$$\mathrm{B}_\pi = \mathrm{BH1} \times \mathrm{BH2} \times \overline{\mathrm{BGC}}(\times \mathrm{BAC}),$$

$$\mathrm{B}_K = \mathrm{BH1} \times \mathrm{BH2} \times \overline{\mathrm{BGC}} \times \overline{\mathrm{BAC}}.$$

The coincidence timing is adjusted on the basis of the flight time of the particles. Protons (anti-protons) can be rejected using the coincidence timing between BH1 and BH2.

2.2. Tracking wire chambers

As described in Sect. 1, the K^- beam intensity is expected to be $\sim 10^6$ [ppp]. With consideration of the kaon purity and decays, the total charged-particle rate is expected to be on the order of several MHz for the downstream trackers and more than 10 MHz for the upstream trackers with the present beam extraction length of ∼2.3 s. In the SKS experiments carried out at the K6 beam line of the 12-GeV proton synchrotron (12GeV-PS) at the KEK Tsukuba Campus, a ∼4 MHz beam was typically used with a 5-mm anode-wire-spacing drift chamber and single-hit TDCs. Thus, the maximum allowed rate per wire was ∼200 kHz.

In the design of the beam spectrometer at J-PARC, we adopted a similar wire chamber configuration but made the anode wire pitch finer than before. We had developed a 1-mm anode-wire-spacing multi-wire proportional chamber (1 mm MWPC) for the upstream tracker and a 3-mm anode-wire-spacing drift chamber (3 mm MWDC) for the downstream tracker. The present configuration of the tracking wire chambers is listed in Table 1. Because of the fabrication schedule, we have adopted the drift chamber used at the K6 beam line (K6 BDC) as BC4[1].

In order to handle a 10-MHz particle rate with the size of $\sim 200^{\mathrm{H}} \times \sim 10^{\mathrm{V}}$ mm^2, a 1-mm anode wire pitch was chosen for the upstream tracker. This pitch size is almost at the technical limit to allow some space for soldering. The gap between the anode and the cathode was determined to be 3 mm from a balance between preventing the discharge and maintaining the gain with a low operation voltage. The anode wire is a gold-plated tungsten wire (with rhenium) with a 15 μm diameter. These anode wires are fixed on the G10 frame with a thickness of 3 mm, which corresponds to the anode–cathode gap. Anode wires exist even outside the window region. The three outermost wires are thicker ones (guard wires) to avoid discharge due to the disarranged field in the edge region. The signal readout lines are drawn out to eight half-pitch connectors, HIROSE FX2-68P-1.27DSL(71), on both

[1] The reversed configuration of BC3 and BC4 is more suitable for reducing the rate per wire. However, the maximum beam rate is limited at the present beam condition, for other reasons.

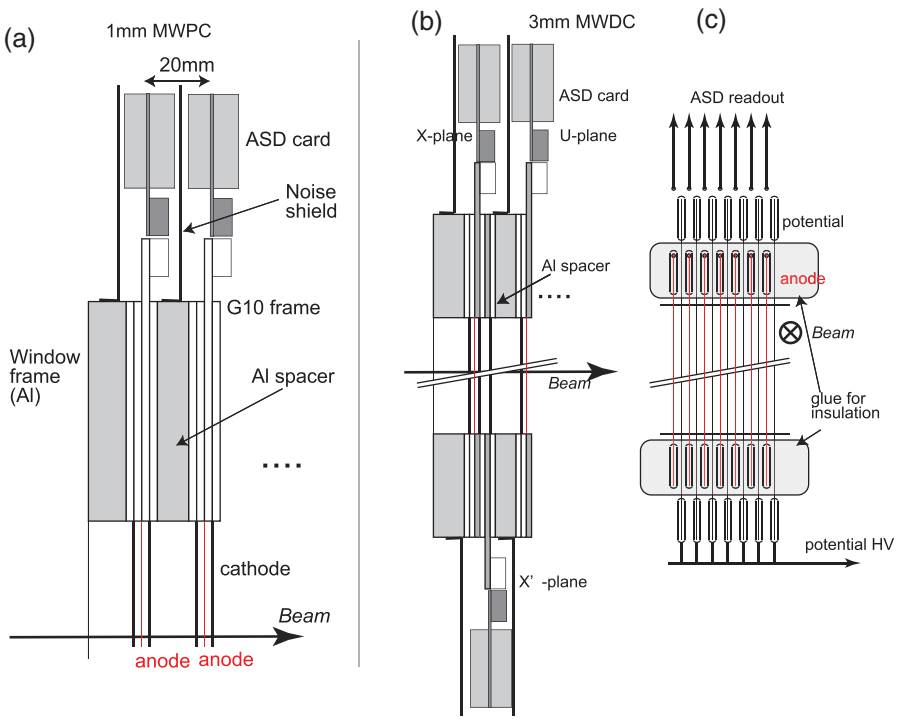

Fig. 4. (a) Structure of the 1 mm spacing MWPC. (b) Side view of the 3 mm spacing MWDC. (c) Front view of the wire frame of the 3 mm spacing MWDC.

the top and bottom of the anode frame. All anode wires are grounded through the readout amplifiers (readout wires) or directly (extended wires). The cathode plate is made of a 12-μm-thick Mylar film coated with 20-μm-thick carbon ink on the anode wire side. The cathode films are also fixed on the G10 frames and connected to an HV line.

The assembled structure of the 1 mm MWPC is shown in Fig. 4(a). The 1 mm MWPC has six layers in an X-U-V-X-U-V configuration, where the X plane measures the horizontal position. The U and V planes are tilted by $\pm 15^\circ$ with respect to the X plane around the beam axis. The distance between the layers is 20 mm, to make a space for ASD cards and noise shields, as shown in the figure.

As a downstream tracker, a 3-mm anode-wire-spacing (1.5 mm drift distance) drift chamber is chosen. The gap between the (anode) wire and the cathode planes is 2.0 mm, which is almost the technical limit of the thickness of the G10 frame: flatness of the frame, especially the gas seal structure. The structure of the 3 mm MWDC is shown in Figs. 4(b) and 4(c). Anode wires of gold-plated tungsten (with rhenium) with a 12.5 μm diameter and potential wires of gold-plated copper–beryllium wire with a 75 μm diameter are fixed alternately with a separation of 1.5 mm on the G10 frame. Since a potential difference of $\sim$1.2 kV exists between the anode and the potential wires, discharge occurs between the potential wires and the soldering pads for anode wires. To avoid this discharge, this area is coated with an epoxy glue for insulation after soldering the wires, as shown in Fig. 4(c). Signal lines are drawn out to the two half-pitch connectors on the top or bottom side. BC3 has six layers in an X-X′-U-U′-V-V′ configuration, where the tilted angles are the same as those in the configuration of the 1 mm MWPC and a prime indicates that the wires are shifted by a half cell to resolve L/R ambiguity. A Mylar film, which is coated with 20-μm-thick carbon ink on both sides, is used for the cathode plate, as some cathode plates are common for two layers.

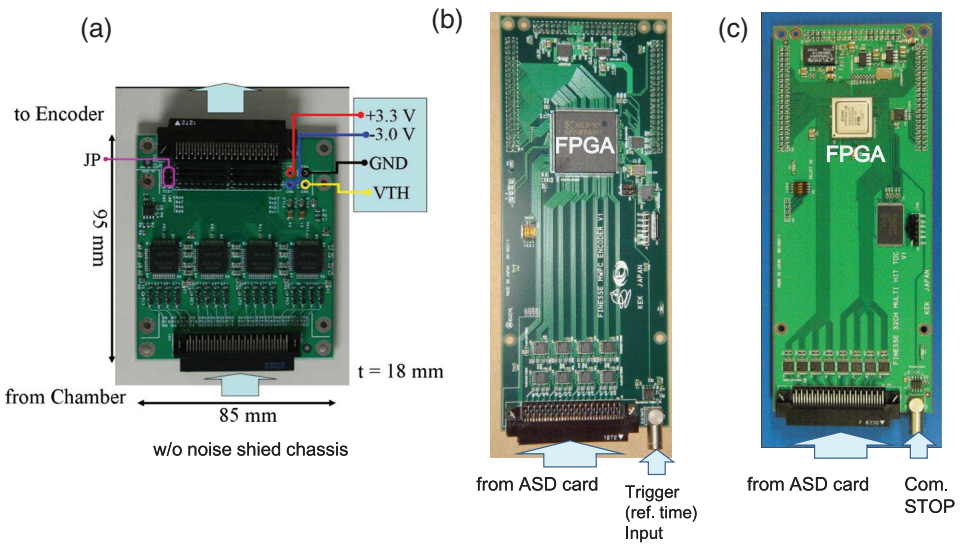

Fig. 5. (a) ASD card for wire chamber readout. (b) MWPC encoder FINNESE board on the COPPER system for the front-end of the MWPC readout. (c) Multi-hit TDC FINNESE board on the COPPER system for the front-end of the drift chamber readout.

BC4 is a drift chamber with an anode spacing of 5 mm and an anode–cathode gap of 2.4 mm, which was originally used at the K6 beam line of 12GeV-PS [2].

2.3. Readout electronics system for wire chambers

The signals are amplified and discriminated by ASD cards connected to the chambers and sent to the front-end modules located in the experimental area for DAQ. The specifications of the 32-channel ASD card are as follows. The input connector is a half-pitch one, HIROSE FX2-68S-1.27DSL, which matches the connector on the chamber. Signals are amplified, shaped, and discriminated by eight ASD chips, which were originally developed for the ATLAS Thin Gap Chamber [11], placed on both sides of the ASD card. Discriminated logic signals of LVDS level are output through a half-pitch connector, KEL 8831E-068-170L-F. Pull-up and pull-down resistors are installed on the card. Power for +3.3 V (0.82 A), −3.0 V (0.11 A), threshold, and ground (GND) are supplied by other cables. A test input signal of NIM logic level can be distributed through the LEMO00 connector on the card. A photograph of the ASD card is shown in Fig. 5(a). The entire card, except for the connectors, is covered with noise shields.

Front-end modules for the chambers were also developed on FINNESE boards of the COPPER system [12] for the MWPC and drift chambers, as shown in Figs. 5(b) and 5(c), respectively. Both modules accept both LVDS and ECL logic signals with a half-pitch connector, KEL 8831E-068-170L-F. The functions are realized by the firmware on the FPGA (Xilinx, Spartan-3 XC3S400 for the MWPC encoder and Vertex-5 family for the multi-hit TDC). Trigger signals (reference time for the MWPC encoder and common stop for the multi-hit TDC) are sent via a LEMO 00 connector on the board or the trigger module on the COPPER system.

The MWPC encoder latches 32 channel input signals (1 or 0) synchronized with the internal 100 MHz clock and sends them to the first FIFO. When the trigger (reference) signal is received, the data that match the time window are sent to the second FIFO for readout. The depth of the first FIFO is 255, which corresponds to the events that occurred within 2.55 μs before the trigger signal. This module functions as a multi-hit TDC with a time resolution of 10 ns and a maximum time range of 2.55 μs.

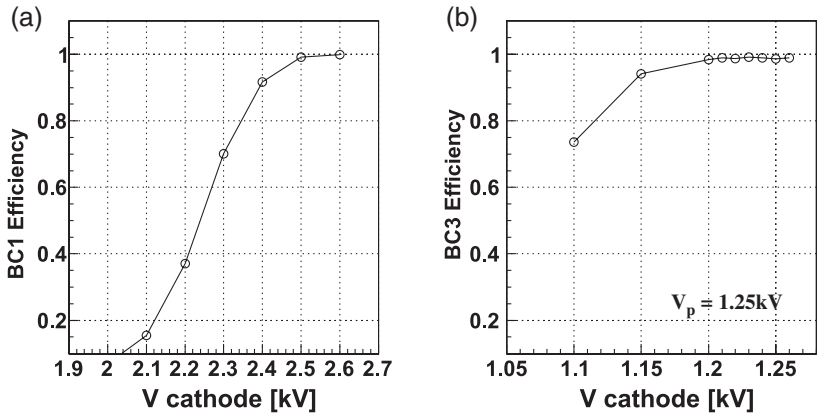

Fig. 6. The measured efficiency curves for BC1 (a) and BC3 (b).

The second FIFO is overwritten by the next trigger. As no data suppression is incorporated, a time window of 30 records (300 ns) was set in normal data-taking.

The multi-hit TDC FINNESE board has a 1-ns resolution and a maximum time range of 65 μs. The depth is 1023 for each channel. Although the development of the modules has been completed, the readout channels available are not sufficient in number. The data from the drift chambers in the beam line (BC3 and BC4) and at the entrance of SKS (SDC1 and SDC2) are currently read out by legacy multi-hit TDC modules on the TKO system.

2.4. Operation of MWPC and MWDC

Figure 6 shows the plane efficiency of one of the 1 mm MWPC (BC1) (a) and the 3 mm MWDC (BC3) (b) layers as a function of the voltage supplied to the cathode plane. The plane efficiency is defined as the ratio of the number of events with more than one hit in the plane to that of well-defined ones where the beam particle was incident in the effective area of the wire chamber. It was measured using a low-intensity pion beam. A gas mixture of Ar(96%)+C_4H_{10}(20%)+methylal(4%) was used for BC1–4 and SDC1 and 2.

In the first E19 run in 2010, the operation voltages were −2.51 kV for BC1 and BC2; −1.23 and −1.25 kV for the cathode plates and the potential wires, respectively, of BC3; and −1.4 kV for both the cathode plates and the potential wires of BC4. These voltages were decided to be optimal at low intensity. Analysis efficiencies for track-reconstruction were approximately 95% and 99% for the entrance (BC1 and BC2) and the exit (BC3 and BC4), respectively, using 1.0×10^6 pions/spill beam, where the spill length was approximately 2.0 s. The discrepancy between the achieved analysis efficiency and the expected one from the plane efficiency for BC1,2 is due to the following reasons. One is a high gas gain operation. The operation current causes a voltage drop at high rate. The other is the bad time structure of the slow extracted beam from the main ring (MR). Due to ripples in the power supplies of MR magnets, the maximum instantaneous beam rate has been up to twenty times as high as the mean rate. Therefore, the plane efficiencies dropped simultaneously for all planes.

In the second E19 run in 2012, we set a slightly lower voltage of −2.47 KV for MWPC. Although the plane efficiency was not 100%, the analysis efficiency was kept to 95% up to 3×10^6 pions/spill beam. Data-taking was carried out using 1.7×10^6 pions/spill beam with 2.2 s spill length. In the above condition, the position resolution of BC3 and BC4 was approximately 0.2 mm (rms) from the residual distributions of the tracking. The position resolution of MWPC is mathematically estimated

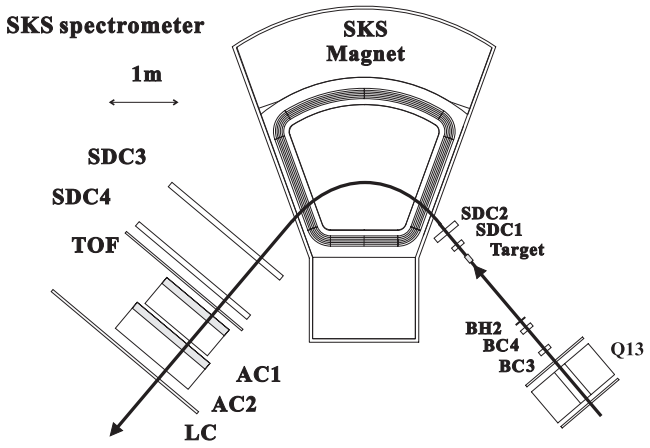

Fig. 7. Setup of SKS in 2010 to carry out the E19 experiment.

to be $1\,\text{mm}/\sqrt{12} \sim 0.3\,\text{mm}$ (rms). This was also confirmed from the residual distributions of the tracking.

3. SKS

SKS [2] was constructed in 1991 at the K6 beam line of 12GeV-PS in KEK. It was in operation from 1991 to 2005 for the purpose of nuclear physics research, such as the spectroscopy of Λ hypernuclei and coincidence experiments with weak decay products or γ-rays from Λ hypernuclei utilizing a high resolution and large solid angle. SKS was moved to J-PARC for further research, with a modification of the magnet's cooling system. Some of the counters were also upgraded to match the requirements of the new experiments at J-PARC.

The spectrometer comprises a superconducting magnet, tracking wire chambers (SDC1–4), and various counters for trigger and particle identification. The detector configuration, including the spectrometer position, may be changed depending on the experiments. Figure 7 shows the spectrometer setup in 2010 for conducting experiments using (π, K) reactions.

3.1. Superconducting magnet

The SKS magnet is a superconducting dipole magnet of the large sector type. The coil is cooled by the pool boiling method. The magnet was originally equipped with a 300-W medium-sized He refrigerator. Because the maximum current of 400 A was low enough and the heat invasion to 4 K was low with 5 W + 1.5 L/h in the original system, the existing 300-W refrigerator could be replaced with small-sized Gifford–MacMahon/Joule–Thomson (GM/JT) cryocoolers to maintain the liquid He level in the steady state. The cooling power of the GM/JT cryocooler is 3.5 W at 4.5 K and 50 Hz, and thus, three GM/JT cryocoolers are needed for the new system. It is emphasized that the recent performance improvements in cryocoolers have made such an application possible.

Figure 8 shows the cryogenic system of the SKS magnet before and after modification. The original coil assembly, which included coils and a coil vessel with the original 2-stage Gifford–MacMahon (GM) cryocooler to cool the coil shield, was reused. An He reservoir to mount three GM/JT and other cryocoolers was newly manufactured and was used as a replacement for the original reservoir. The conventional copper current leads were replaced with Bi2223 HTC current leads with a new 1-stage GM cryocooler (54 W at 40 K) for reducing the heat leakage from the leads. An additional dedicated

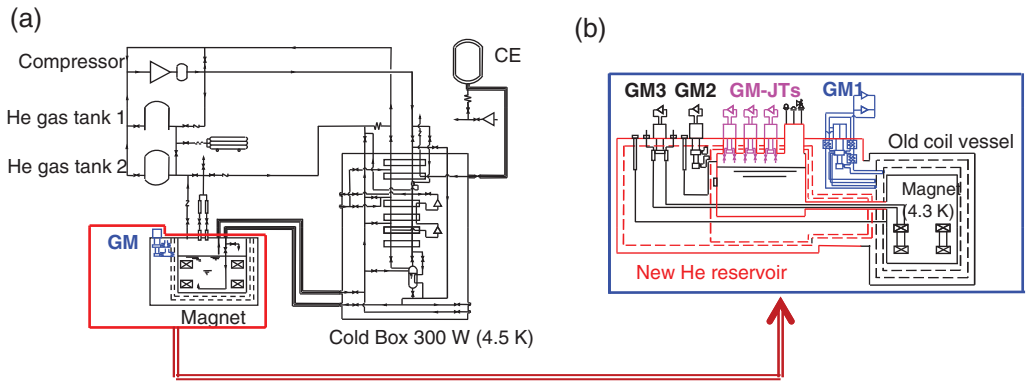

Fig. 8. Cryogenic system of the SKS magnet before (a) and after (b) modification.

2-stage GM cryocooler to cool the GM/JT insert port was installed to enhance the performance of GM/JT cryocoolers.

During the modification of the cooling system, a fault took place in the innermost part of the coil, which was unfortunately impossible to repair. Thus, 330 turns out of 2108 turns in the coil were bypassed, resulting in a lowered maximum magnetic field of 2.48 T at 400 A. The field shape, especially at the pole edge and near the coil, was also changed. Therefore, a calculated field map needs to be used in the momentum analysis, instead of the precisely measured field maps that were used in the analysis of previous experiments at the K6 beam line.

The magnet is located at the K1.8 area in the Hadron Hall 6.4 m underground, while all compressors, the magnet power supply, and the control system are located in the machine room on ground level. The compressors and cryocoolers on the He reservoir of the magnet are connected with 40 m flexible tubes. As the new cryogenic system has no control valve, the main roles of the control system are monitoring temperatures, pressures, liquid levels, strain gauges etc., interlocking, and alarming.

As the new cryogenic system cannot by itself cool the magnet from room temperature to 4.3 K, the magnet was cooled down to 120 K by liquid N_2 (2500 L) and to 4.3 K by liquid He (10 000 L). In total, 1.5 months were needed to cool down the magnet, from August 18 to October 2 2010. The magnet was successfully energized on October 14. The magnetic field in the central region is measured by NMR. The measured excitation curve was reproduced by a finite element method calculation within 1.5%. The measured magnetic field is recorded during the data-taking period. The parameters of the magnet are listed in Table 2. Technical details of the cryogenic system are provided in another report [13].

3.2. Trigger and particle identification counters

The scattered particles, i.e. kaons in the present setup, are identified by a combination of three kinds of trigger counters: a time-of-flight wall (TOF), aerogel Čerenkov counters (AC1 and AC2), and a lucite Čerenkov counter (LC). While the TOF is sensitive to all charged particles, AC1 and AC2 are only sensitive to pions (+ electrons/positrons) and the LC to pions and kaons (+ electrons/positrons) in the momentum range of interest (0.7–1.0 GeV/c).

The TOF is a horizontally segmented plastic scintillator located downstream of the tracking wire chamber (SDC4). The size of each segment is $70^{\mathrm{H}} \times 1000^{\mathrm{V}} \times 30^{\mathrm{T}}$ mm^3. While the number of segments used in the previous experiments at KEK was 15, it was increased to 32 in order to cover the wider momentum acceptance for the J-PARC experiments. The signals of each segment are detected

Table 2. SKS magnet parameters before and after modification.

Item	Before	After
Max. current	498 A 400 A (after 1994)	400 A
Inductance	90.3 H at 498 A	78.4 H at 400 A
Stored energy	11.3 MJ at 498 A	6.3 MJ at 400 A
Dumping resistance	3 Ω	2 Ω
Refrigerators	Medium-sized (300 W at 4.5 K) +1 GM	3 GM/JTs (3.5 W × 3 at 4.5 K) +3 GMs
Stored liquid He	106 L for coil 50 L for He reservoir	106 L for coil 300 L for He reservoir
Heat invasion to 4 K	3 W + 1.5 L/h (before 1994) 5 W + 1.5 L/h (after 1994)	6–8 W
Total weight	280 tons	282 tons

by fast phototubes (H1949) on the top and bottom sides. The TOF measures the time-of-flight from BH2 and identifies the scattered particle combined with momentum and flight path length information in the offline analysis. The measured time-of-flight resolution between BH2 and TOF was 150 ps (rms), which is enough to separate the scattered pions, kaons, and protons.

The LC, a threshold-type Čerenkov counter, is installed at the most downstream end of the spectrometer. It is segmented into 28 pieces horizontally. Each piece has dimensions of $100^{\mathrm{H}} \times 1400^{\mathrm{V}} \times 40^{\mathrm{T}}\,\mathrm{mm}^3$ and two phototubes (H1949) on the top and bottom sides. The size of the LC was extended from 14 segments to 28 in order to increase the momentum acceptance of the spectrometer. In the acrylic radiator, a wavelength shifter, bis-MBS, is mixed by 10 ppm by weight to radiate photons uniformly, in order that the detection efficiency does not depend on the incident angles. On the other hand, due to the wavelength shifter, a considerable percentage of protons are detected even below the threshold of 0.85 GeV/c.

AC1 and AC2 are threshold-type Čerenkov counters with silica aerogel radiators having a thickness of ∼113 mm and a refractive index of 1.05. These counters were used in the previous experiments at KEK. The effective areas of AC1 and AC2 are $1050^{\mathrm{H}} \times 1200^{\mathrm{V}}\,\mathrm{mm}^2$ and $1400^{\mathrm{H}} \times 1400^{\mathrm{V}}\,\mathrm{mm}^2$, respectively. Čerenkov photons are detected by 18 (AC1) and 20 (AC2) 3-inch phototubes on the left and right sides. The number of photo-electrons was typically ∼6 over the entire area for 0.85 GeV/c pions. AC1 and 2 are installed between the TOF and LC.

Since the beam operation in February 2012, AC1 and AC2 have been replaced by a large-sized aerogel Čerenkov counter (LAC), which was fabricated based on the radiators and phototubes of AC2, to fit the size of the TOF and the LC. The effective area is $2080^{\mathrm{H}} \times 1200^{\mathrm{V}}\,\mathrm{mm}^2$. The size of the LAC in the beam direction is 70 cm, whereas the size of AC1 and AC2 is 50 cm. The photons are detected by 30 phototubes.

The following logic defines the scattering particles at the trigger level:

$$\mathrm{S}_\pi = \mathrm{TOF} \times \mathrm{LC},$$

$$\mathrm{S}_K = \mathrm{TOF} \times \mathrm{LC} \times \overline{\mathrm{AC}},$$

where

$$\mathrm{AC} = \mathrm{AC1} \times \mathrm{AC2}, \text{ or}$$

$$= \mathrm{LAC}.$$

In addition to the logic above, a matrix coincidence logic between the segments of the TOF and LC can be applied in the trigger. The matrix logic is made not by the conventional NIM modules but

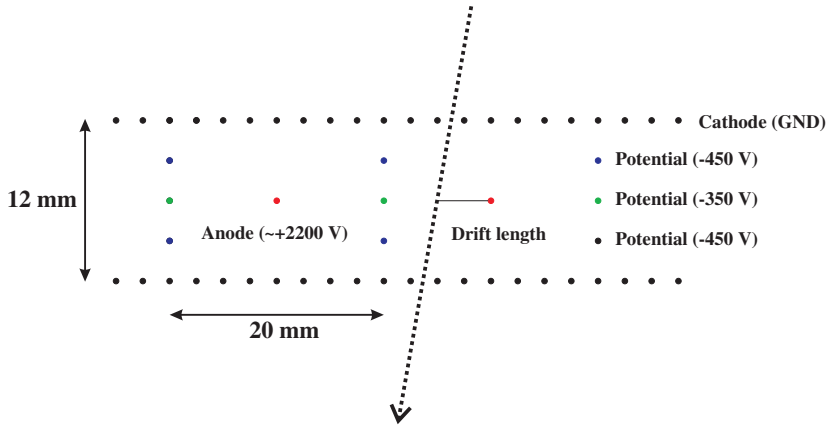

Fig. 9. Cell structure of SDC3 and SDC4.

by a FPGA module, TUL-8040 [14]. The logic is programmable and can be generated with a delay of 20 ns. The matrix coincidence logic trigger was effective in suppressing the background triggers and reducing trigger rates in the first and second physics runs of E19, in which the beam hit the coil vessel and caused a lot of background triggers.

3.3. Tracking drift chambers

At the entrance of the SKS magnet, two sets of newly fabricated drift chambers (SDC1 and SDC2) are installed. SDC1 is the same as BC3 except that it has four planes in a V-V'-U-U' configuration. SDC2 has a similar structure to BC3. However, the anode–anode spacing and anode–cathode gap of SDC2 are 5 mm and 2.5 mm, respectively. The readout electronics for SDC1 and SDC2 are the same as those for BC3. The position resolution for these chambers was approximately 0.2 mm (rms).

Large-sized drift chambers (SDC3 and SDC4) are installed at the exit of the magnet. These chambers, which had been used in the BNL-AGS experiments [15], were moved to J-PARC with the aim of increasing the momentum acceptance. The effective area is $2140^{H} \times 1140^{V}$ mm^2, twice as large as the length of the previous ones at KEK. Each chamber has six layers in a V-X-U-V-X-U configuration, where the U and V wires are tilted by $\pm 30^\circ$ with respect to the X wires.

All anode wires were replaced with gold-plated tungsten wires with a 25 μm diameter, increased from the original 20 μm diameter for more strength. The drift length is 10 mm, and its cell structure is shown in Fig. 9. Both the potential and cathode wires are gold-plated copper–beryllium ones with an 80 μm diameter. The cathode wires, the pitch of which is 2 mm, are grounded, while a negative voltage for the potential wires and positive voltage for the anode are applied in the operation. The HV lines were also modified so that the operation can be partly turned off for the beam area according to the experimental conditions. The signals from the anode wires of SDC3 are amplified by the boards on the chamber and discriminated by the modules housed in a VME crate. On the other hand, those of SDC4 are both amplified and discriminated by the boards on the chamber. The timing signals are sent to the K1.8 counting house on ground level and digitized by the single-hit TDCs (Dr.T II on the TKO system).

Figure 10 shows the efficiencies as a function of the anode voltage measured for a low-intensity π beam with an Ar(50%)+C_2H_6(50%) gas mixture. The operation voltage was set to $+2.2$ kV for the anode and -450 and -350 V for the potential wires as shown in Fig. 9, in the E19 run. A tracking efficiency of 99.8 ± 0.2% and a position resolution of 0.2 mm (rms) were achieved.

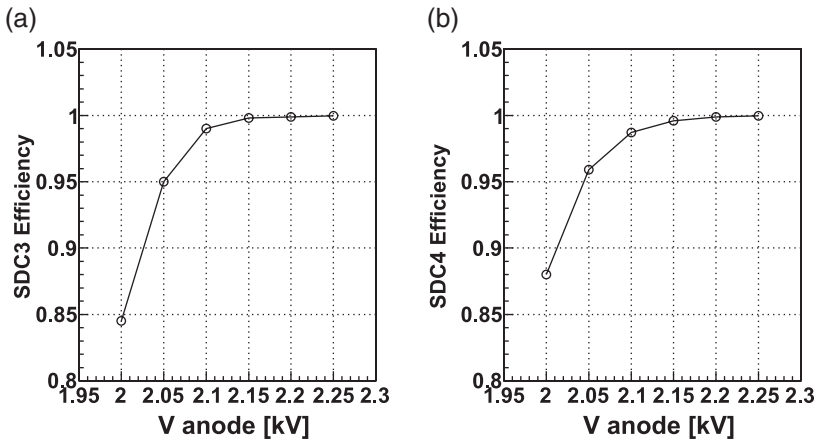

Fig. 10. Efficiency curve of one of the SDC3 (a) and SDC4 (b) layers as a function of the anode wire voltage.

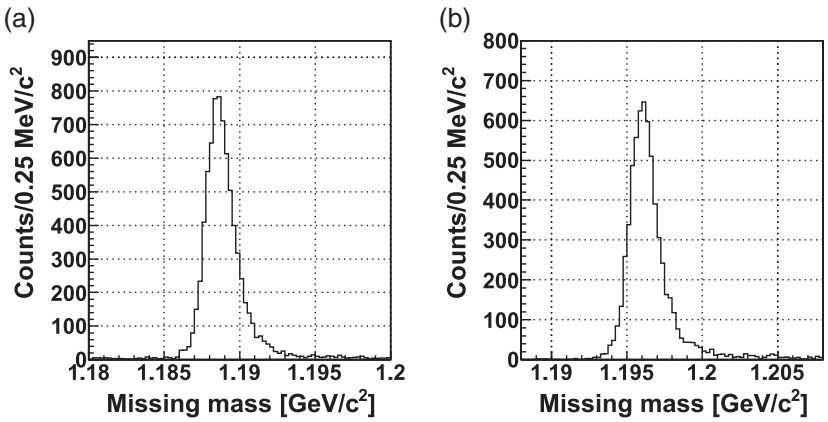

Fig. 11. Missing-mass spectra for $p(\pi^+, K^+)\Sigma^+$ (a) and $p(\pi^-, K^+)\Sigma^-$ (b) reactions at 1.37 GeV/c.

3.4. Resolution of the spectrometer system

The momentum of the scattered particle is determined by reconstructing the trajectory from the hit positions of SDC1–4. Prior to full trajectory reconstruction, the hit positions are selected by tracking with a straight line, locally at the entrance (SDC1 and SDC2) and exit (SDC3 and SDC4) of the magnet. Next, full reconstruction is carried out with a fast Runge–Kutta method [16] using a magnetic field map. The flight path length, which is necessary for particle identification, is also determined. From the momentum vectors obtained from both the beam and SKS spectrometers, the reaction vertex point, scattering angle, and, finally, missing mass can be calculated.

As mentioned previously, we had to use a calculated magnetic field map instead of the measured one. Therefore, it was very important to check the spectrometer resolution. For this and other purposes, we measured the $p(\pi^\pm, K^+)\Sigma^\pm$ reactions using a 12-cm-long liquid hydrogen target at 1.37 GeV/c. Kaons were measured with SKS at 2.48 T. A missing-mass resolution of 1.9 ± 0.1 MeV/c^2 (FWHM) was obtained for both reactions as shown in Fig. 11. The missing-mass resolution is mainly determined by the momentum resolution of the scattered particles of 2.0×10^{-3} (FWHM). A tail in the high mass side is considered to be due to the Landau tail of the energy loss in the target.

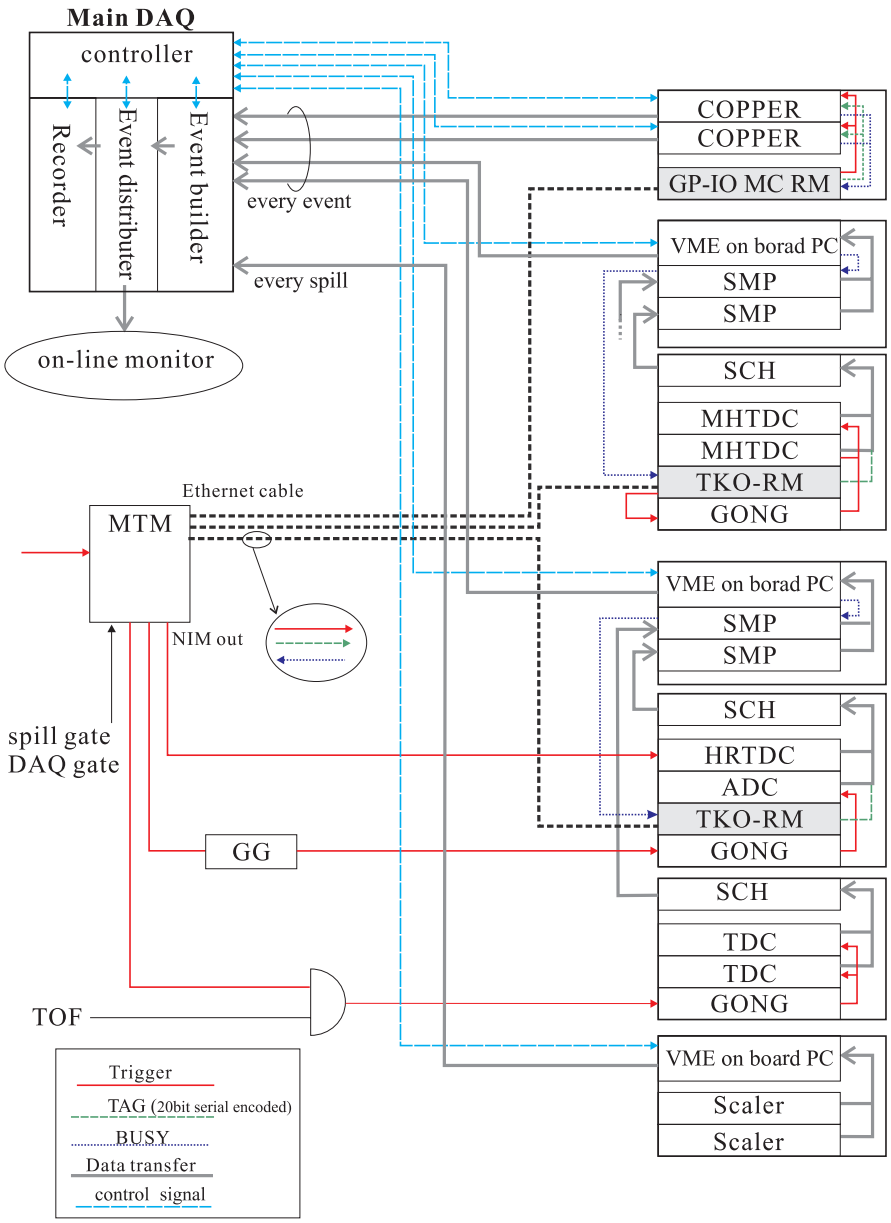

Fig. 12. Diagram of the data acquisition system.

4. Data acquisition system

Figure 12 shows a diagram of the DAQ system. Several kinds of conventional subsystems, such as VME and TKO, and a new network-based COPPER system [12] are used to effectively utilize the previous resources.

The raw signals of the trigger counters are digitized with ADC and TDC modules in a TKO crate in the counting house. The timing signals from SDC3 and 4 are digitized with the single-hit TDC (Dr.T II) modules in TKO crates in the counting house, while those from other drift chambers (BC3, BC4 and SDC1, SDC2) are digitized with multi-hit TDC (MHTDC) modules in TKO crates in the experimental area. The digitized data on the TKO modules are transferred to the VME-SMP (super memory partner) in the VME crate by the event trigger. The data are read out by the CPU board on the VME crate and transferred to the DAQ host computer via an Ethernet connection.

The signals from MWPCs (BC1 and BC2) are digitized with the MWPC encoder FINNESE modules on the COPPER system in the experimental area. One COPPER board houses four FINNESE boards and has two Ethernet ports (one port is in use for our application). Therefore, in the COPPER system, 128-channel data can be transferred to the DAQ host computer in parallel.

Readout and transfer of these data are done event-by-event by the normal event trigger. The scaler data for counts of the trigger counters, numbers of requested and accepted triggers, etc., recorded by VME scaler modules are read out and transferred to the DAQ host computer by both the normal trigger and the special one at the spill-end.

As several kinds of subsystems are located in different places (propagation delay of $\sim$500 ns), synchronization of events such as busy handling and distribution of the event-tag and triggers are important. We have developed a trigger and event-tag distribution system [17]. This system includes master trigger module (MTM) and receiver modules (RM) for the COPPER, TKO, CAMAC, and VME subsystems. The MTM receives *Trigger Request* from the trigger logic and generates *Trigger Accept* after busy handling, then distributes the trigger signal and an event-tag to the RMs on each node via a serial data-link for the event-tag and a wire for the trigger timing using two category-7 Ethernet cables. The event-tag has two numbers, an event number and a spill number. The event number is incremented by *Trigger Accept*. The spill-end signal also generates *Trigger Accept* and distributes the trigger and event-tag to the RMs. These numbers can be reset using a Reset signal or RUN Start input. On each subsystem, data from the modules and the event-tag are processed by the event trigger from the RM. A *Busy* signal is sent to the RM when the system cannot accept the event trigger.

A new piece of network-based DAQ software [17] has also been developed. The **Event-Builder** process on the DAQ host computer collects data fragments from each node, builds the data structure by checking the consistency using the event-tag, and sends these data to the **Event-Distributor**. The **Event-Distributor** distributes the event data to the **Recorder** and **Online Monitor** programs. The **Recorder** process receives all data and records them to the data storage. The **Controller** controls all the processes on the DAQ host computer and DAQ nodes. Since a TCP/IP connection is used on both the control and data links , these processes can be run on different host computers.

5. Summary

In summary, a high-resolution spectrometer system for both beams and scattered particles has been constructed at the K1.8 beam line at the Hadron Experimental Facility of J-PARC for spectroscopy experiments on hypernuclear and strangeness physics. The beam spectrometer with a *QQDQQ* configuration has been designed with a momentum resolution of 3.3×10^{-4} (FWHM) in first-order optics calculations. Beam trackers, a 1 mm anode wire spacing MWPC and a 3 mm anode wire spacing MWDC, as well as a readout system for them, have been newly developed. The scattering particle spectrometer, SKS, which was used for a long time at the K6 beam line of 12GeV-PS at the Tsukuba Campus, has been transferred to J-PARC with modifications of the cryogenic system with the aim of using small-sized GM/JT and GM cryocoolers. The counters and tracking wire chambers have also been replaced with larger ones in order to increase the momentum acceptance. A new network-based DAQ system and trigger and event-tag distribution system have been developed to use many kinds of DAQ subsystems, both legacy ones, TKO and VME, and a new COPPER system.

The performance of the spectrometer system has been confirmed in the commissioning run and the first physics run of the E19 experiment. A time-of-flight resolution of $\sim$140 ps, good enough to separate kaons and pions, has been obtained for the beam spectrometer. A missing-mass resolution of 1.9 ± 0.1 MeV/c^2 (FWHM) has been obtained for the $p(\pi^{\pm}, K^{+})\Sigma^{\pm}$ reactions.

Acknowledgements

We would like to thank those staff members at J-PARC who are not listed in the author list, for their implicit co-operation in the construction and operation of the spectrometer system. We wish to thank Professor Taniguchi for his advice on noise reduction of the chamber readout system. Most of the detectors and their readout systems were constructed or modified with support from a Grant-in-Aid for Scientific Research on Priority Areas, "Multi-Quark System with Strangeness" (Nos. 17070001, 17070003, 17070006).

References

[1] K. Agari et al., "Secondary Charged Beam Lines", submitted to Prog. Theor. Exp. Phys.
[2] T. Fukuda et al., Nucl. Instrum. Methods Phys. Res., Sect. A **361**, 485 (1995).
[3] J-PARC Proposal P05, http://j-parc.jp/NuclPart/pac_0606/pdf/p05-Nagae.pdf.
[4] J-PARC Proposal P10 (revised), http://j-parc.jp/NuclPart/pac_0701/pdf/P10-dcx.pdf.
[5] J-PARC Proposal P19, http://j-parc.jp/NuclPart/pac_0606/pdf/p19-Naruki.pdf.
[6] J-PARC Proposal P13, http://j-parc.jp/NuclPart/pac_0606/pdf/p13-Tamura.pdf.
[7] J-PARC Proposal P18, http://j-parc.jp/NuclPart/pac_0606/pdf/p18-Bhang.pdf.
[8] J-PARC Proposal P22, http://j-parc.jp/NuclPart/pac_0701/pdf/P22-weak.pdf.
[9] K. Shirotori et al., Phys. Rev. Lett. **109**, 132002 (2012).
[10] T. Takahashi (on behalf of the Hadron Beamline Group and the K1.8 Experimental Group), Nucl. Phys. A **835**, 88 (2010).
[11] O. Sasaki and M. Yoshida, IEEE Trans. Nucl. Sci. **46**, 1871 (1999).
[12] Y. Igarashi et al., IEEE Trans. Nucl. Sci. **52**, 2866 (2005).
[13] K. Aoki et al., Proceedings of the Twenty-Third International Cryogenic Engineering Conference and International Cryogenic Materials Conference 2010, (2011) pp. 965–970.
[14] Web site: http://lambda.phys.tohoku.ac.jp/∼takahasi/TUL-8040.
[15] R. W. Stotzer et al., Phys. Rev. Lett. **78**, 3646 (1997).
[16] J. Myrheim and L. Bugge, Nucl. Instrum. Methods **160**, 43 (1979).
[17] Y. Igarashi et al., IEEE Trans. Nucl. Sci. **57**, 618 (2010).